# Towards Foundation Models for Experimental Readout Systems Combining Discrete and Continuous Data

## J. Giroux $^{1,\star}$ , C. Fanelli $^{1,\star}$

- <sup>1</sup> William & Mary, Department of Data Science, Williamsburg, VA 23185, USA
- \* Author to whom any correspondence should be addressed.

E-mail: jgiroux@wm.edu, cfanelli@wm.edu

8 June 2025

#### Abstract.

We present a (proto) Foundation Model for Nuclear Physics, capable of operating on low-level detector inputs from Imaging Cherenkov Detectors at the future Electron Ion Collider. To address limitations in existing next-token prediction approaches—namely resolution loss from VQ-VAE tokenization and lack of conditional generation—we propose three key innovations: (i) separate vocabularies for discrete spatial features and continuous variates, combined via Causal Multi-Head Cross-Attention (CMHCA), (ii) continuous kinematic conditioning through prepended context embeddings, and (iii) scalable and simple, high-resolution continuous variate tokenization without joint vocabulary inflation. Our model enables fast, high-fidelity generation of pixel and time sequences for Cherenkov photons, validated through closure tests in the High Performance DIRC. We also show our model generalizes to reconstruction tasks such as pion and kaon identification, in which we show its ability to leverage fine-tuning.

**Keywords:** Foundation Models, Causal Cross Attention, Transformers

#### 1. Introduction

Foundation Models (FM) are beginning to emerge as powerful tools within the field of both Nuclear Physics (NP) and High Energy Physics (HEP), supporting the inclusion of multiple downstream tasks [1–4] and fine-tuning [5,6]. Seminal works, such as those in [2,3], show that relatively modest sized transformer backbones are easily generalizable to both reconstruction (particle identification (PID), jet tagging, etc) and simulation tasks. In which fine tuning from one task to another possess inherent reduction in computational overhead in comparison to models trained from scratch. Moreover, they show that different

<sup>&</sup>lt;sup>1</sup>In [2], the authors coin the term proto-Foundation Models, representing model development along the path to true, large-scale Foundation Models.

underlying mechanisms, i.e., next token prediction, masked prediction (akin to traditional decoder only, or encoder-decoder style language models) [1, 2, 6–8] or iterative refinement through Diffusion Transformers [9] can be equally as generalizable. In which the latter method [3] promotes reconstruction tasks through selective time restrictions in the diffusion processes (i.e., t=0). In general, both of these approaches work with relatively highlevel reconstructed quantities such as 4-vectors. Recently, Birk et al. [10] demonstrated that next-token prediction can be effectively applied to simulate calorimeter response, particularly for modeling photon-induced shower development using low-level features such as pixel positions and energy depositions. While the results are promising and represent an important step forward, there are two potential limitations in the current approach that warrant further consideration. First, given the requirements of next token prediction to (generally) operate in a discrete space, quantization methods must be employed upstream in terms of a learnable tokenization process, generally in the form of a Vector Quantised-Variational AutoEncoder (VQ-VAE) [11]. VQ-VAE models provide discrete latent encodings, therefore allowing tokenization of continuous and multidimensional spaces such as location (pixel) and energy in calorimeters. While powerful, such methodologies do not come without significant tradeoffs in terms of resolutions - a potential degrading effect in physics simulations of detectors through loss of information. Second, their approach does not encompass conditional generation, and therefore generative tasks that exhibit explicit conditional dependence on external parameters (e.g., Cherenkov production in DIRC detectors) is not possible. As a result, we propose two improvements for next token prediction models to circumvent these potential issues in physics, in which we deploy our techniques to Imaging Cherenkov Detectors at the future Electron Ion Collider (EIC) pixelated detectors that require both precise location, and timing information of individual hits.<sup>3</sup> The main contributions of our work is as follows:

- We introduce a (proto) Foundation Model in Nuclear Physics, operating on low level detector inputs. Its performance is demonstrated through a series of closure tests using Cherenkov detectors at the future EIC.
- We introduce learning through split vocabularies in space and time, in which discretization (tokenization) in the continuous time space can be done at a fraction of the resolution of the detector. These modalities are combined through Causal Multi-Head Cross-Attention (CMHCA) [12, 13] to produce spatio-temporally aware embeddings, in which we query the pixel space given times.
- We introduce continuous kinematic dependencies through fixed context, in which prepending of kinematic embeddings drives sequence generation forward in time. Providing kinematic aware next token prediction.

The use of split vocabularies allows our model to retain high resolution time generations, without the need for excessive vocabulary size or learnable tokenization.

<sup>&</sup>lt;sup>2</sup>Decoded tokens inherently posses some uncontrolled smearing effect proportional to the codebook size.

<sup>&</sup>lt;sup>3</sup>We leave translation to calorimeters (see, e.g., [10]) for future works.

In fact, the resolutions capable of being deployed in our study would comprise a joint-vocabulary (space and time) of roughly 36 million tokens (5920 possible time values, 6144 possible pixel values). We also note that our approximation through split vocabularies remains valid under most pixelated detector systems, given the one-to-many mappings that occur between space and the continuous variate such as time, energy or both [14]. In this scenario, one could envision the combination of space, time, and energy through sequential CMHCA blocks, where time queries energy to generate a temporal-energy informed embedding, which is then used to query spatial indices.

In what follows, we demonstrate the ability of our method to produce high fidelity fast simulation of pions and kaons in the High Performance DIRC (hpDIRC) through a series of closure tests, along with ability to operate under a classification scheme both with and without fine tuning.

#### 2. Dataset

We utilize the dataset developed by Giroux et al. [15], which records Cherenkov photon hit patterns captured by the hpDIRC readout system comprised of photomultiplier tube (PMT) arrays. Each hit pattern is associated with a single charged particle track, which is inherently characterized by kinematic parameters. As depicted in Figure 1, an individual track produces a sparse and inherently stochastic subset of hits (highlighted in red). However, when aggregating hits from multiple tracks with identical kinematics—namely, momentum ( $|\vec{p}|$ ) and polar angle ( $\theta$ )—a well-defined probability density function (PDF) emerges. Importantly, the number of hits per track is not fixed, and dependent on the kinematics, resulting in a combinatorially large space of possible hit configurations. This variability presents a significant modeling challenge for autoregressive (AR) architectures.

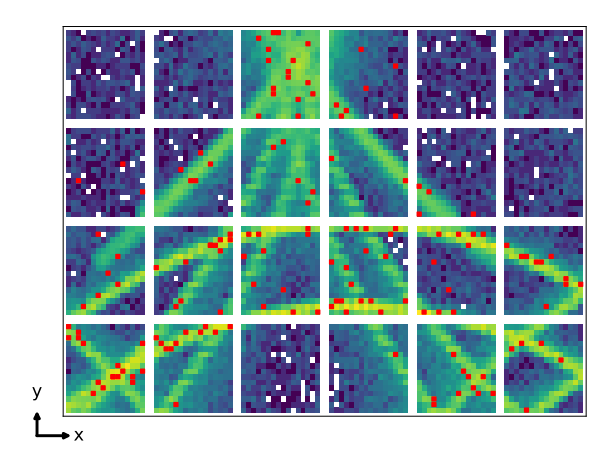


Figure 1: **Optical box output:** Individual tracks leave sparse hit patterns (red points) integrated over time on the hpDIRC readout plane. The denser hit pattern is obtained by accumulating multiple tracks with the same kinematics. Figure and caption taken from [15].

As stated in [15], the generated charged tracks (both pions and kaons) are distributed

approximately uniformly over the phase-space, spanning  $1 < |\vec{p}| < 10 \text{ GeV/c}$ ,  $25 < \theta < 160^\circ$ , providing  $\sim 5$  million tracks for each PID. We limit ourselves to a max sequence length of 250, corresponding to a large range in photon yields across the phase-space. In contrast to prior works learning information at the photon-level, in which tracks can be formed through aggregation, we instead directly learn to generate individual tracks (sequences of hits). As a result, the transformations in [15] are not needed given that we directly work with the discretized readout (pixel indices) and time.

#### 3. Methods

#### Tokenization of Space and Time

Given the pixelated nature of the readout system, no additional tokenization is required along the spatial dimension; each discrete pixel index corresponds uniquely to a fixed (x, y) coordinate in the PMT array, yielding a spatial vocabulary size of 6144. In regards to time, which is a continuous variate, we employ a simple linear binning strategy in which we discretize on the order of 1/4 the time resolution yielding a vocabulary of size 5920. While we employ uniform binning in this work, more sophisticated schemes—such as non-linear binning or function-based discretizations—could be used to capture known nonlinearities in the readout system. We also observed that further reducing the temporal resolution to one-tenth of the intrinsic resolution had negligible impact on model performance. Therefore, our current choice of 1/4 the timing resolution provides similar vocabulary sizes for both spaces

#### Time Queries Space

We first obtain time and spatial embeddings through learnable, independent projections from their vocabularies, in which we add positional embeddings along each dimension. We also embed both the momentum and angular values through independent linear projections (continuous spaces), and prepend our kinematics as initial context along both time and spatial projections, an example of which is given in Eq. 1. Each embedding dimension is set to 256 in our experiments.

$$\operatorname{spatial} \to \{ |\vec{p}|, \theta, \operatorname{SOS}_p, p_1, \dots, p_n, \operatorname{EOS}_p \}$$
$$\operatorname{time} \to \{ |\vec{p}|, \theta, \operatorname{SOS}_t, t_1, \dots, t_n, \operatorname{EOS}_t \}$$
(1)

We then combine information through a transformer block using CMHCA, in which we obtain our Query projection (Q) from the time embeddings, and the Key (K) and Value (V) projections from the spatial embeddings.<sup>4</sup> The result is a spatio-temporally aware embedding to be further processed by transformer blocks utilizing traditional Multi-Head Self-Attention (MHSA) blocks [16]. Each transformer block consists of its respective attention type with 8 heads, a linear projection layer, and a standard feed forward network with 2 linear layers and GeLU activation [17]. Given the large combinatorial space of

<sup>&</sup>lt;sup>4</sup>For a given time, query the possible pixel locations of valid Cherenkov photons.

plausible tracks at a given kinematics, careful consideration must be taken within each attention head. Specifically, we must enforce the model to learn more focused attention maps given an initial context. We do not want the attention maps to simply collapse to the most probable configurations as aggregations over the entire phase-space. Therefore, we employ multiple normalization schemes, in which both pre and post norm strategies are used. We further augment this through normalization of the Q,K matrices [18], in which  $\ell_2$  normalization is applied with a learnable scale factor. This makes attention scores invariant to their scale - promoting stability, increased variability in our output space and direction focused. This being a key feature given the large combinatorial space of plausible track configurations mentioned prior.

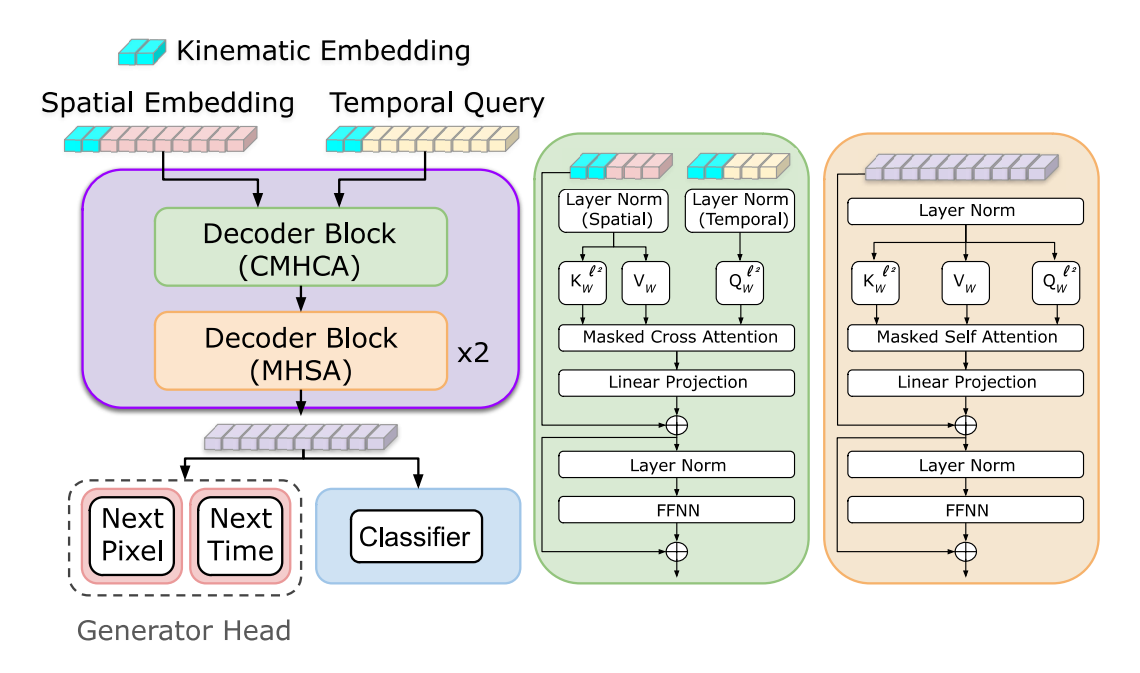


Figure 2: Architecture: Spatial and temporal sequences are first independently embedded via learnable projections from their respective vocabularies, with positional encodings added along each dimension. Kinematic information (momentum magnitude and polar angle) is projected from continuous space and prepended as contextual tokens to both sequences. The time embeddings serve as queries (Q), while the spatial embeddings provide keys (K) and values (V) within a Causal Multi-Head Cross Attention (CMHCA) mechanism. The resulting spatio-temporal representations are passed through transformer blocks utilizing Multi-Head Self Attention (MHSA). We apply both pre- and post-normalization schemes, including  $\ell_2$ -normalized Q and K projections with learnable scaling. For generation, the model outputs next-token predictions over space and time vocabularies through two linear heads. For classification, a CLS token is used to summarize the sequence and predict class scores via a final linear layer. FFNN stands for Feedforward Neural Network.

In the case of generation, the final output from the transformer blocks feeds two independent next token prediction heads operating over the space and time vocabularies. Each of which are represented by single linear layers. In the case of classification, we represent our output latent distributions through a single linear layer. This layer is fed through a traditional *CLS* token format, in which we place this token at the start of each sequence. A diagrammatic representation of our model is shown in Fig. 2.

In our current study, we deploy two separate generative models for the two classes, pions and kaons  $(\pi/K)$ , as motivated by previous works and also their high degree of similarity as momentum increases. The latter requiring clear separation of their modes to provide high fidelity, and reliable simulation. We leave their combination under one model for future studies.

## 4. Analysis and Results

#### Generative Model Evaluation

We follow the procedure in Giroux et al. [15], validating our fast simulation approach at the central region in momentum  $(6 \,\mathrm{GeV/c})$  through a series of histograms and ratios, in which we will also compare the learned sequence length, *i.e.*, ability to learn correct photon yield as a function of the phase-space. Plots for additional kinematics  $(e.g., 3 \,\mathrm{GeV/c})$  and  $(e.g., 3 \,\mathrm{GeV/c})$  can be found in Appendix A and Appendix B. Note that while our model directly provides pixel and timing location, we convert the spatial indices into  $(e.g., 3 \,\mathrm{GeV/c})$  coordinates to provide more informative visualizations. This will then be followed by a closure test using classifier metrics, namely the same Kernel Density Estimation (KDE) derived from FastDIRC [19] at fixed momentum. In which we ultimately translate the fidelity of our generations into a more interpretable metric of separation power.

Histogram Level Evaluations We begin through visual comparisons of generations produced by our architecture to the ground truth of GEANT4 at fixed momentum. We show generations from our model near the two ends of the bar (large, or small polar angle), along with the central region of the bar. As mentioned in [15], the former provides insight into our architectures ability to capture symmetry in ring structures at the extreme polar angles, while accounting for the inherent time shift that occurs due to path length differences. The latter provides insight into the ability of the architecture to model both direct, and indirect photons emitted from central regions of the bar, indicated through multi-modal structures in time. In general, smaller values of the polar angle provide insight into the ability to model both indirect and direct photons. However, in the central region the number of indirect and direct photons tends to be more similar and motivates our choice. While not quantitative in nature, fixed point generation comparisons are extreme stress tests of our model given its training on a fully continuous phase space. Moreover, these simple projections provide immediate cues into potential mode collapse, and deviation from correct rings structures.

In the generations that follow, we employ a Nucleus Sampling [20] technique with p=0.995, and a fixed temperature of T=1.05. These generations schemes have shown to provide the most consistent cumulative distributions across the phase-space. It should

also be noted that given the high degree of stochasticity within individual sequences, small changes in these parameters can result in significantly different outputs. In fact, the idea of "next token" prediction of Cherenkov photons is highly ambiguous, as shown by previous works in which high fidelity track-level generations can be produced through aggregations of individual photon generators [15,21]. In these works, the authors show treating individual photons as independent of one another provides no loss of coherence. Fig. 3 depicts generations of kaons (left column of images) and pions (right column of images) for various polar angles (30° top row, 95° middle row and 150° bottom row).

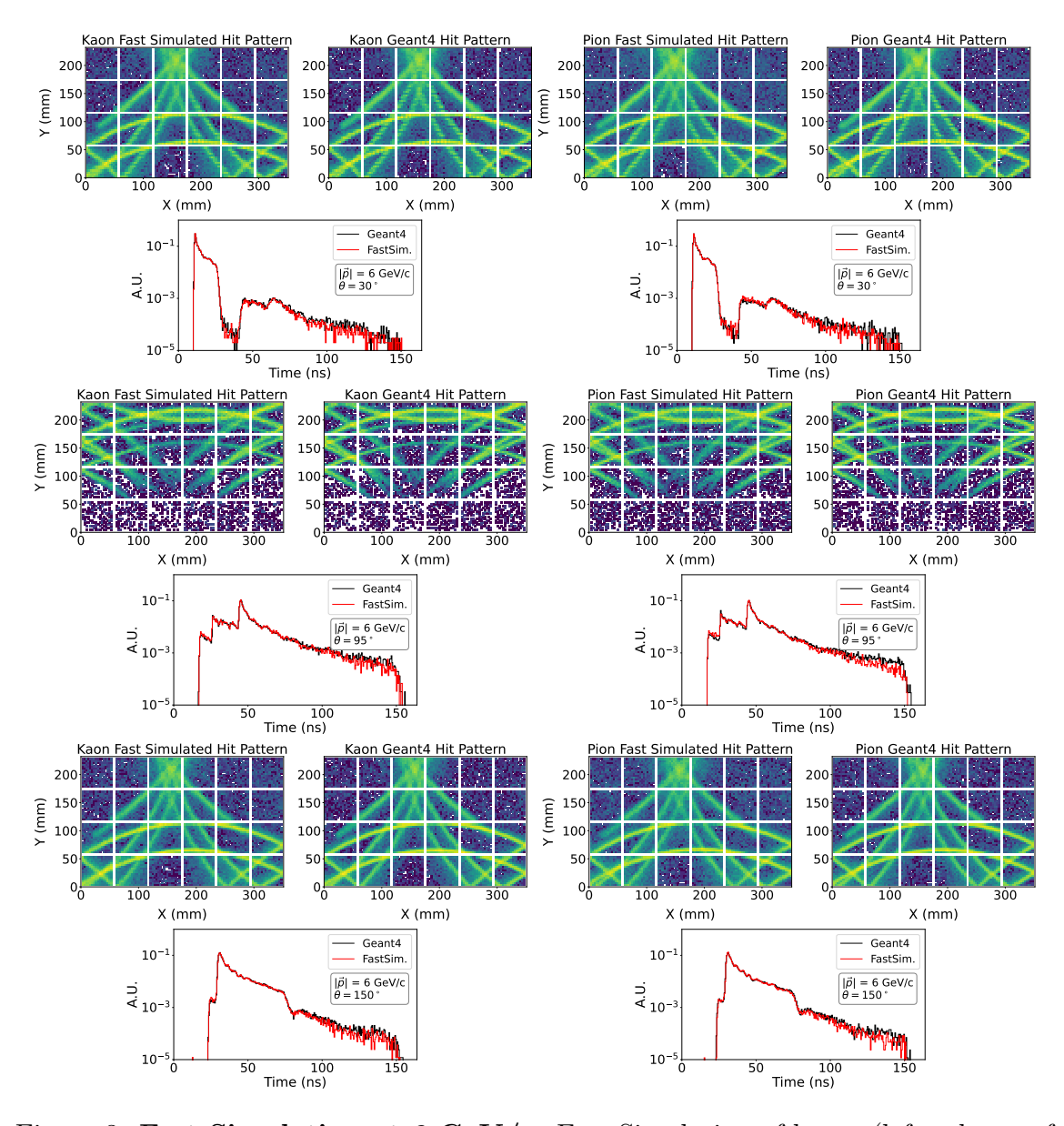


Figure 3: **Fast Simulation at 6 GeV/c:** Fast Simulation of kaons (left column of plots), and pions (right column of plots) at 6 GeV/c and various polar angles, using Nucleus sampling and fixed temperature.

From inspection of the figure, we can qualitatively assess that our model correctly captures kinematic dependencies in both space and time. Furthermore, we are able to obtain hints of geometrical effects, such as the kaleidoscopic effect [22] at angles closer to the expansion volumes  $(e.g., 30^{\circ})$ . Prior fast simulation methods have been unable to capture such details. This will be discussed in more detail in later sections. To provide a more qualitative assessment of our generations, we provide cumulative distributions in Fig. 4, for (a) kaons and (b) pions.

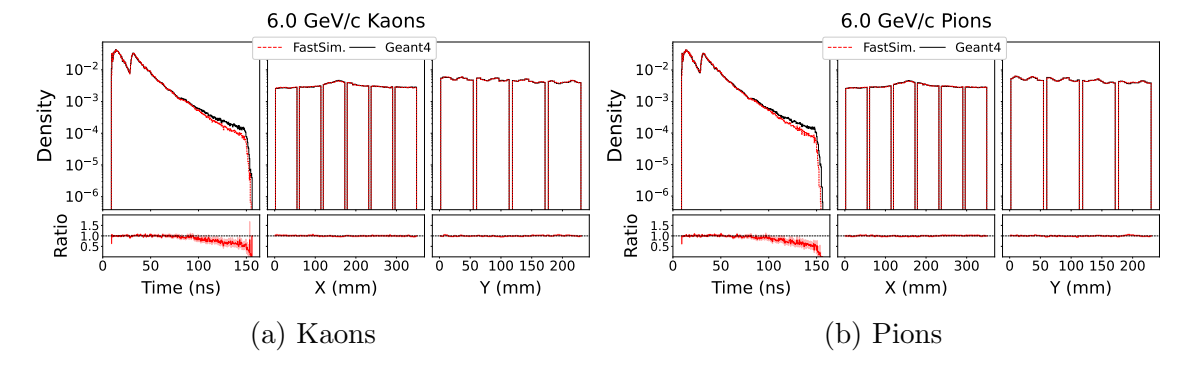


Figure 4: Ratio Plots at 6 GeV/c: Ratio plots for kaons (top) and pions (bottom), using Nucleus sampling and fixed temperature.

We note exceptional agreement in the spatial dimensions, in which our ratios are  $\sim 1$  across all values. Our time distribution is in high agreement with the ground truth along the main population (most Cherenkov hits are within the first 100 ns), although the tails of the distribution tend to struggle due to low density. This is an expected outcome in the context of modern generative models in general.

Unlike previous fast simulation methods for Cherenkov detectors, in which post-hoc modeling of the photon yield must be employed, our method directly learns this variability

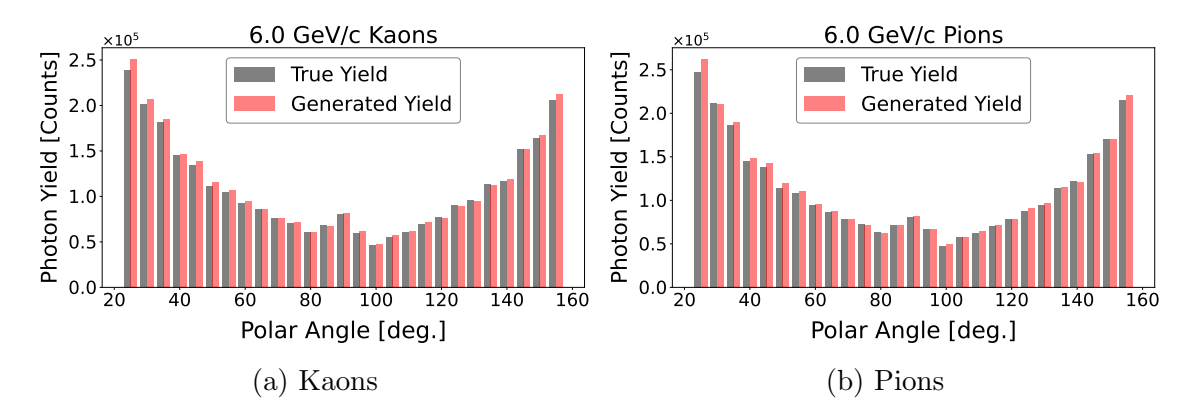


Figure 5: **Photon Yield Comparison at 6 GeV/c:** Comparison of generated photon yield for kaons (top) and pions (bottom), using Nucleus sampling and fixed temperature.

in sequence length as a function of the phase-space. Fig. 5 depicts a comparison between the generated and ground truth photon yields at 6 GeV/c, in  $5^{\circ}$  bins of the polar angle for (a) kaons and (b) pions.

We note good agreement for both generative models (pions and kaons) in terms of photon yield, with slight over estimation at lower values of the polar angle (e.g.,  $\theta < 100^{\circ}$ ). These results are consistent at all regions of the phase-space as indicated by plots in Appendix A and Appendix B.

KDE based Evaluation We again follow the methods devised in [15], translating fidelity measurements to a more interpretable metric of separation power using the KDE method of FastDIRC.<sup>5</sup> This evaluation is performed at fixed momenta—specifically 3 GeV/c and 6 GeV/c—to emphasize fidelity testing at specific kinematic points, which serves as a stringent stress test for our generative models trained over a fully continuous kinematic space. Fig. 6 depicts the performance comparison for  $3 \, \text{GeV}/c$  (top) and  $6 \, \text{GeV}/c$  (bottom), for various values of the polar angle (in bins of 5°), with fixed sized reference populations of 800k, for GEANT4, NF, and our proposed method (indicated in legend).

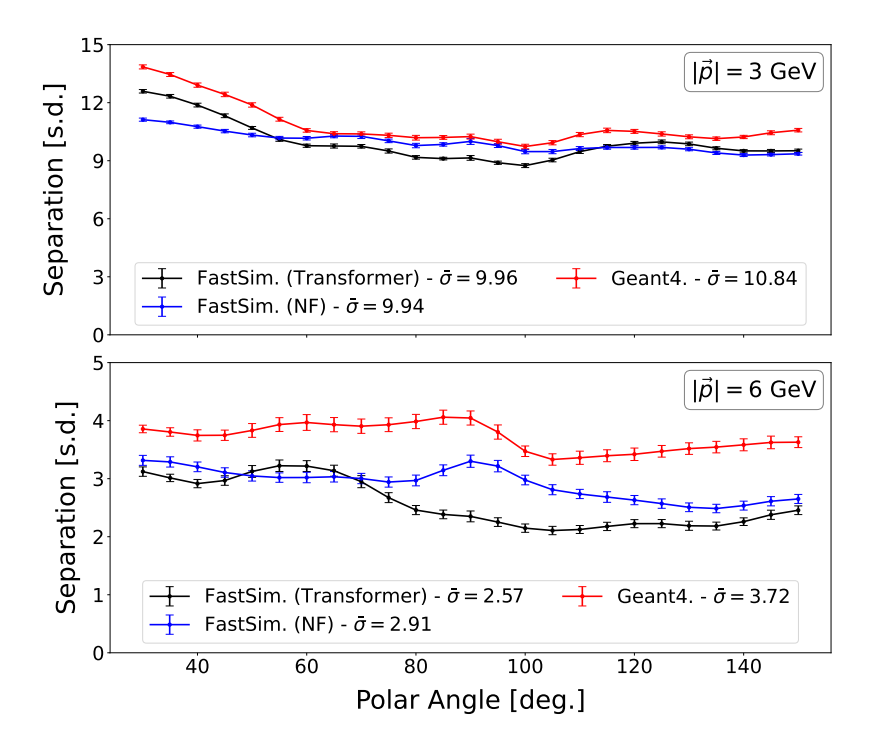


Figure 6: **KDE Performance Comparison:** Particle Identification performance of pions and kaons using FastDIRC KDE method with Geant4 reference populations, and fast simulated populations from Normalizing Flows and our method (Transformer-based) at 3 GeV/c (top) and 6 GeV/c (bottom) for various values of the polar angle.

<sup>&</sup>lt;sup>5</sup>More information on the exact formulation of the metric, and underlying process can be found in [15].

From inspection of the figure, we initially see that our proposed method does degrade in performance in comparison to both Geant4, and previously proposed methods such as NF. As pointed out in [15], any smoothing of the underlying probability distribution produced by our model will incur significant performance decreases in comparison to GEANT4 given the ring structures only differ by a few pixels spatially at higher momentum (eventually converging at large enough momentum). In contrast to NF, the smoothing effect incurred is not inherent to the method, but rather an artifact of the data itself. Specifically, there is approximately uniform uncertainty at each forward step in time translating to a highly ambiguous space of "next token" prediction, i.e., relatively flat attention scores. Given the inherent uncertainty in our data as to which is the most optimal next hit, different sampling techniques possess the ability to greatly alter our generations - arguably more than other AR models operating in the traditional domain of language. In light of this, we observe that post-hoc optimization can be employed to further curate generated samples. While not specifically fine tuning weights, optimizing generation parameters (e.q., temperature, dynamic temperature, p values, etc) can improve fidelity and is left for future studies.<sup>6</sup>

Geometric Effects As discussed earlier, given that our model operates in a discrete space, we are able to capture geometric effects (degree varies with angle and sampling method) such as the kaleidoscopic effect. The kaleidoscopic effect manifests as appeared "pixel preferences" in the readout system, with the effect being more pronounced the closer a track hits to the expansion volume. Fig. 7 depicts generations at the closest possible polar angle to the expansion volume ( $\theta = 25^{\circ}$ ), for both (a) NF, and (b) our AR approach in the figure referenced as 'Transformer'.

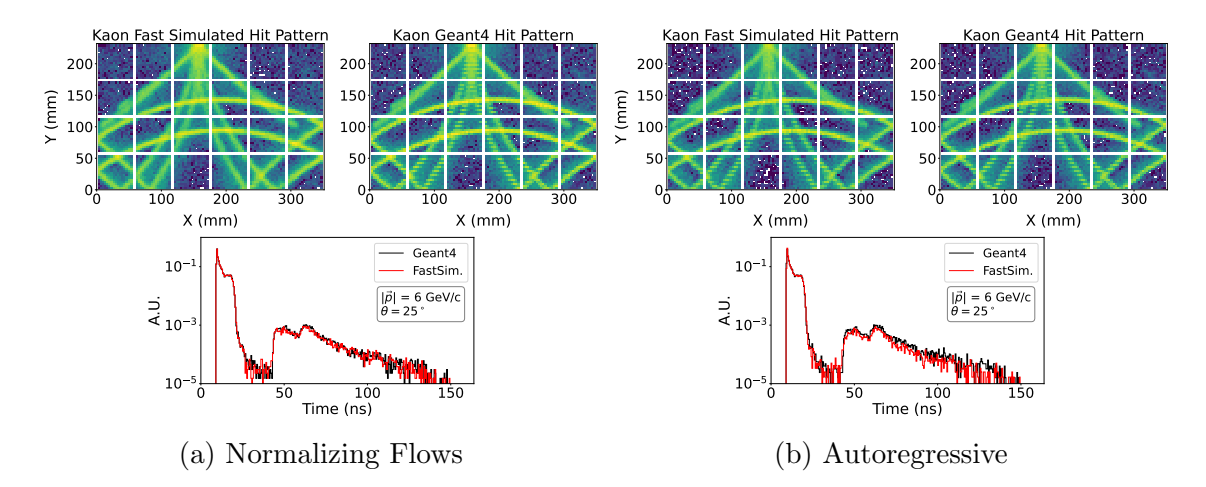


Figure 7: Geometrical Effect Comparison at 6 GeV/c: Comparison of (a) Normalizing Flows and (b) our Auto-regressive approach in their ability to capture geometrical effects.

<sup>&</sup>lt;sup>6</sup>We have implemented and tested a wide variety of sampling methods, see https://github.com/wmdataphys/FM4DIRC for more details.

While promising, further research into the capacity of our model is required to fully capture this effect at all regions of the phase-space.

## Particle Identification and Fine-tuning

As shown in previous works [2,3], the flexible structure of transformer backbones supports various downstream tasks (primarily fast simulation and reconstruction tasks such as PID). In what follows, we show the performance of our model, in which we fine-tune our backbone structure (essentially all transformer blocks) from a generative procedure, to one of sequence-level classification. Specifically, we classify if charged tracks originate from pions or kaons within our detector. We also show that fine-tuning our models from generation to classification provides inherent speed ups in convergence, along with slight performance increases. Fig. 8 (a) shows the performance of our model in terms of separation power at 3 Gev/c (top), and 6 Gev/c (bottom) and various values of the polar angle. We also provide performance comparisons using the NF models from [15], and the DLL method devised in [21]. The average separation power over the polar angle is reported in the legends. Fig. 8 (b) shows the accuracy of our model integrated over the phase-space as a function of training iteration (number of batches), for both fine-tuned and models trained from scratch.

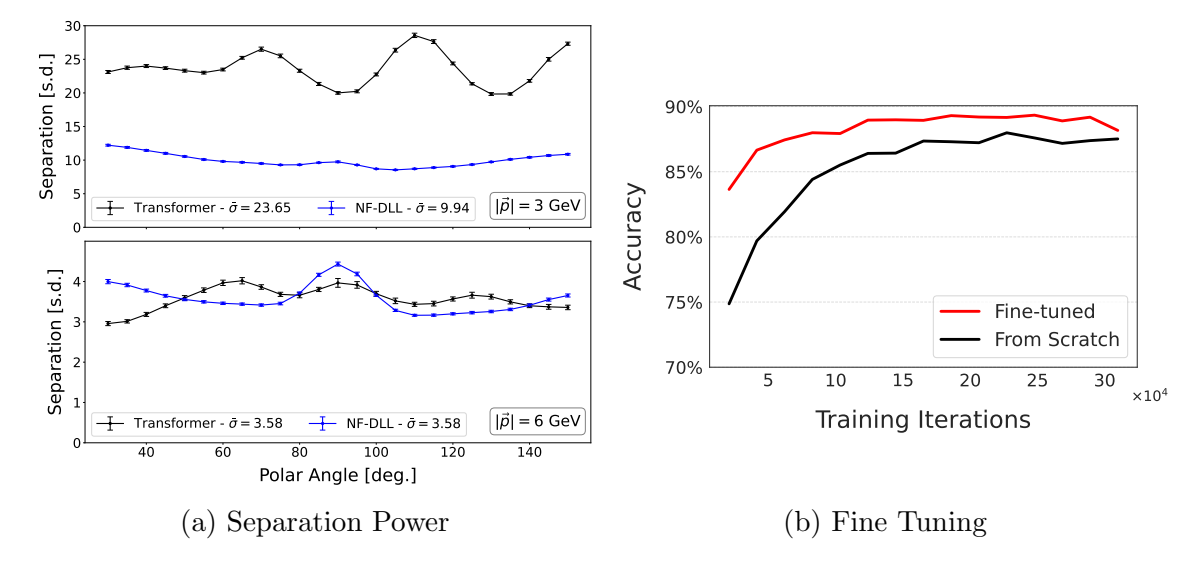


Figure 8: Particle Identification Performance Comparison: PID performance of pions and kaons using (a) Normalizing Flow Delta-Loglikelihood (NF-DLL) method, and our method at 3 GeV/c (top) and 6 GeV/c (bottom) for various values of the polar angle, and (b) comparison of accuracy versus training iterations for models trained from scratch, and fine-tuned integrated over the entire phase-space.

From inspection of Fig. 8 (a) we conclude that both NF, and our FM are able to surpass required separation power of  $3\sigma$  at  $\sim 6 \,\text{GeV}/c$ , as outlined in the EIC Yellow Report [23]. We also note the unique differences in their performance, in which our FM

is more heavily impacted by changes in polar angle as depicted by higher non-uniformity (e.g.), see separation power at 3 GeV/c). A potential artifact of model configuration, or perhaps method of kinematic conditioning. With inspection of Fig. 8 (b) we show our model is capable of fine-tuning, it benefits in terms of both computational efficiency (rate of convergence), and slightly increases in accuracy. We also note the algorithm's clear ability to separate charged pion and kaons at 3 Gev/c, in which our separation power essentially doubles in contrast to NF. While impressive, the usefulness of such separation power at low momentum is debatable and preferred elsewhere at higher momentum where the particle identification becomes more challenging. In future studies we aim to shift some of the focus the model puts on this momentum region through momentum weighted training schemes, or trainings limited to higher impact kinematic ranges to allow increased performance.

#### 5. Summary and Conclusions

With this work, we have introduced a (proto) Foundation Model working on low-level input features (*i.e.*, pixelated readout systems) for Nuclear Physics applications. We have shown through a series of closure tests that our model is capable of performing both generative, and reconstruction tasks in which we are able to leverage fine-tuning to increase computational efficiency.

In the case of generative modeling, our discretized approach in space allows potential for capturing low-level geometric effects seen in DIRC detectors, an advancement over prior methods [15]. Moreover, we have introduced a method in which we alleviate the need for excess quantization over continuous domains, allowing the physical sensor resolutions of detectors to be respected through adjacent vocabularies. Our method fuses spatial and temporal information through Causal Multi-Head Cross Attention (CMHCA), yielding temporally aware spatial embeddings that are subsequently processed using standard transformer blocks. We believe this architecture is both flexible and broadly applicable to a variety of detector systems, including calorimeters. Given the inherent stochasticity in physical readout systems, the concept of a many-to-many mapping approximated through split vocabularies may offer promising results.

We have also demonstrated that our model achieves the desired separation power  $(3\sigma \text{ at } 6 \text{ GeV/c})$  for charged pion and kaon identification, with performance comparable to or exceeding that of other Deep Learning methods. Interestingly, our Foundation Model exhibits greater sensitivity to variations in polar angle, which may reflect its internal representation of detector geometry or the nature of its kinematic conditioning. Additionally, we find that fine-tuning not only accelerates convergence but also yields slight gains in classification accuracy. Notably, the model demonstrates excessively strong discriminative power at lower momenta—though the practical importance of such performance may be limited. To better align model focus with experimental priorities, future studies will explore momentum weighted, or limited phase-space training strategies that emphasize high-impact kinematic regions.

Despite the encouraging performance observed, further refinement of our method is necessary to enable higher-fidelity simulation and improved classification performance, particularly at higher momentum. As seen in Large Language Models, emergent capabilities often arise as a function of scale. Accordingly, we intend to investigate the scalability of our approach through detailed ablation studies focused on both model capacity and the volume of training data.

Lastly, we aim to assess the model's ability to fine-tune across experiments, with particular interest in the GLUEX DIRC and the hpDIRC at the future EIC. While differences in production mechanisms and detector geometries exist between GLUEX and the EIC, we hypothesize that the underlying physics governing DIRC detectors remains sufficiently invariant to enable effective cross-experiment fine-tuning.

## Code Availability

The code is publicly available at https://github.com/wmdataphys/FM4DIRC.

## Acknowledgments

We thank William & Mary for supporting the work of JG and CF through CF's startup funding. The authors acknowledge William & Mary Research Computing for providing computational resources and technical support that have contributed to the results reported within this article.

#### References

- [1] Finke T, Krämer M, Mück A and Tönshoff J Learning the language of QCD jets with transformers 2023 Journal of High Energy Physics **2023** 1–18
- [2] Birk J, Hallin A and Kasieczka G Omni Jet- $\alpha$ : the first cross-task foundation model for particle physics 2024 Machine Learning: Science and Technology **5** 035031
- [3] Mikuni V and Nachman B OmniLearn: A method to simultaneously facilitate all jet physics tasks 2024 arXiv preprint arXiv:2404.16091
- [4] HEP-JEPA: A foundation model for collider physics
- [5] Vigl M, Hartman N and Heinrich L Finetuning foundation models for joint analysis optimization in High Energy Physics 2024 <u>Machine Learning</u>: <u>Science and Technology</u> 5 025075
- [6] Golling T, Heinrich L, Kagan M, Klein S, Leigh M, Osadchy M and Andrew Raine J Masked particle modeling on sets: towards self-supervised high energy physics foundation models 2024 Machine Learning: Science and Technology 5 035074
- [7] Huang A, Melkani Y, Calafiura P, Lazar A, Murnane D T, Pham M T and Ju X A language model for particle tracking 2024 arXiv preprint arXiv:2402.10239
- [8] Butter A, Huetsch N, Schweitzer S P, Plehn T, Sorrenson P and Spinner J Jet diffusion versus JetGPT Modern networks for the LHC 2025 SciPost Phys. Core 8 026
- [9] Peebles W and Xie S 2023 Scalable diffusion models with transformers Proceedings of the IEEE/CVF international conference on computer vision pp 4195–4205
- [10] Birk J, Gaede F, Hallin A, Kasieczka G, Mozzanica M and Rose H OmniJet- $\{\alpha_C\}$ : Learning point cloud calorimeter simulations using generative transformers 2025 <u>arXiv preprint</u> arXiv:2501.05534
- [11] Van Den Oord A, Vinyals O <u>et al.</u> Neural discrete representation learning 2017 <u>Advances in</u> neural information processing systems **30**
- [12] Lin H, Cheng X, Wu X and Shen D 2022 CAT: Cross Attention in Vision Transformer 2022 IEEE international conference on multimedia and expo (ICME) (IEEE) pp 1–6
- [13] Fei J, Li D, Deng Z, Wang Z, Liu G and Wang H Video-ccam: Enhancing video-language understanding with causal cross-attention masks for short and long videos 2024 <u>arXiv</u> preprint arXiv:2408.14023
- [14] Ameli F, Battaglieri M, Berdnikov V V, Bondí M, Boyarinov S, Brei N, Celentano A, Cappelli L, Chiarusi T, De Vita R et al. Streaming readout for next generation electron scattering experiments 2022 The European Physical Journal Plus 137 958
- [15] Giroux J, Martinez M and Fanelli C 2025 Generative Models for Fast Simulation of Cherenkov Detectors at the Electron-Ion Collider (arXiv:2504.19042)
- [16] Vaswani A, Shazeer N, Parmar N, Uszkoreit J, Jones L, Gomez A N, Kaiser Ł and Polosukhin I Attention is all you need 2017 Advances in neural information processing systems 30
- [17] Hendrycks D and Gimpel K Gaussian error linear units (GeLUs) 2016 (arXiv:1606.08415)
- [18] Henry A, Dachapally P R, Pawar S and Chen Y Query-key normalization for transformers 2020 (arXiv:2010.04245)
- [19] Hardin J and Williams M FastDIRC: a fast Monte Carlo and reconstruction algorithm for DIRC detectors 2016 J. Instrum. 11 P10007 (arXiv:1608.01180)
- [20] Holtzman A, Buys J, Du L, Forbes M and Choi Y The curious case of neural text degeneration 2019 (arXiv:1904.09751)
- [21] Fanelli C, Giroux J and Stevens J Deep (er) reconstruction of imaging Cherenkov detectors with swin transformers and normalizing flow models 2025 Machine Learning: Science and Technology 6 015028

- [22] Dey B et al. Design and performance of the Focusing DIRC detector 2015 Nucl. Instrum. Methods Phys. Res. A 775 112–131 (arXiv:1410.0075)
- [23] Khalek R A <u>et al.</u> Science requirements and detector concepts for the electron-ion collider: EIC yellow report 2022 Nuclear Physics A **1026** 122447

# Appendix A. Evaluation at $3 \,\mathrm{GeV}/c$

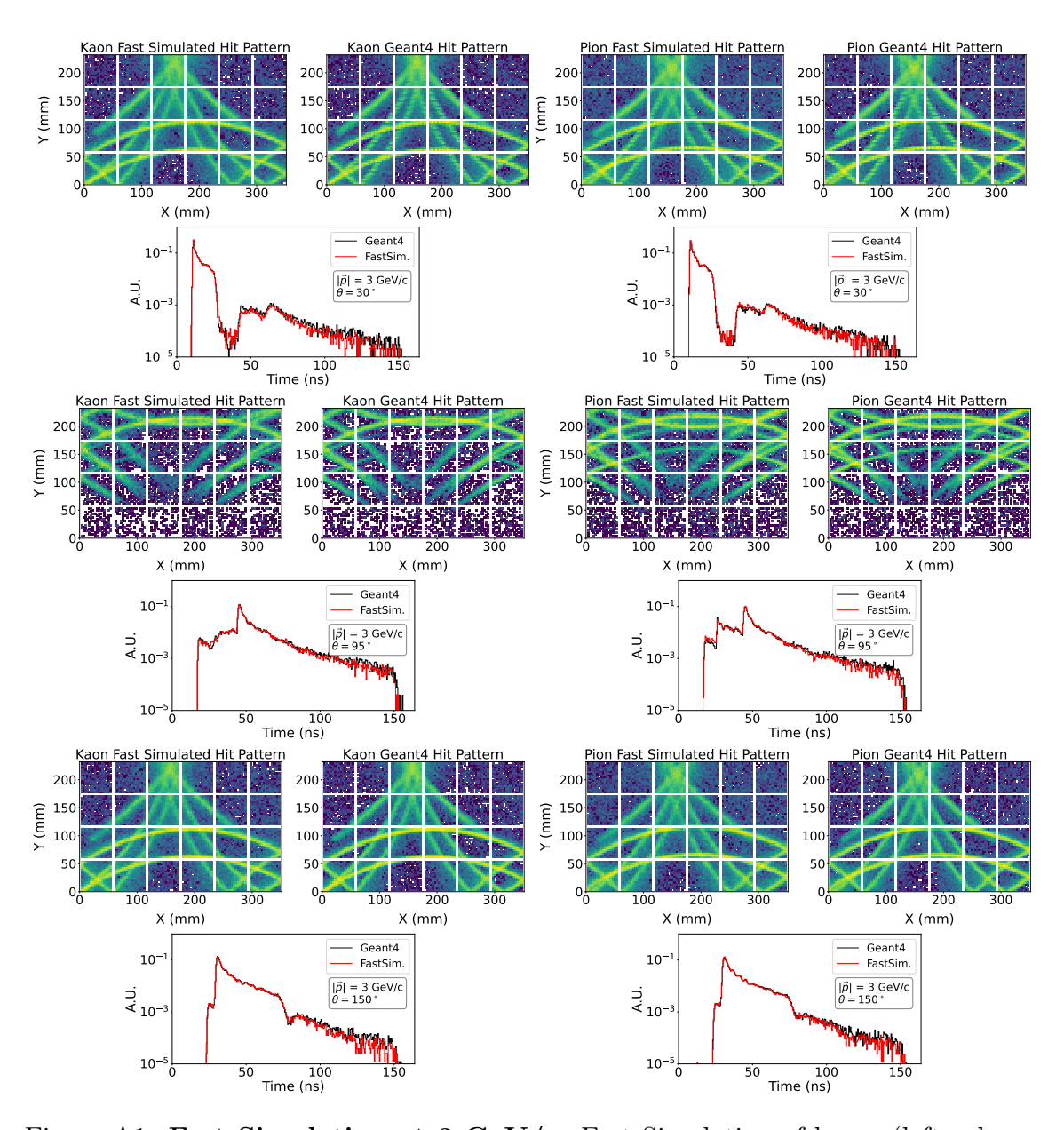


Figure A1: **Fast Simulation at 3 GeV/c:** Fast Simulation of kaons (left column of plots), and pions (right column of plots) at 3 GeV/c and various polar angles, using Nucleus sampling and fixed temperature.

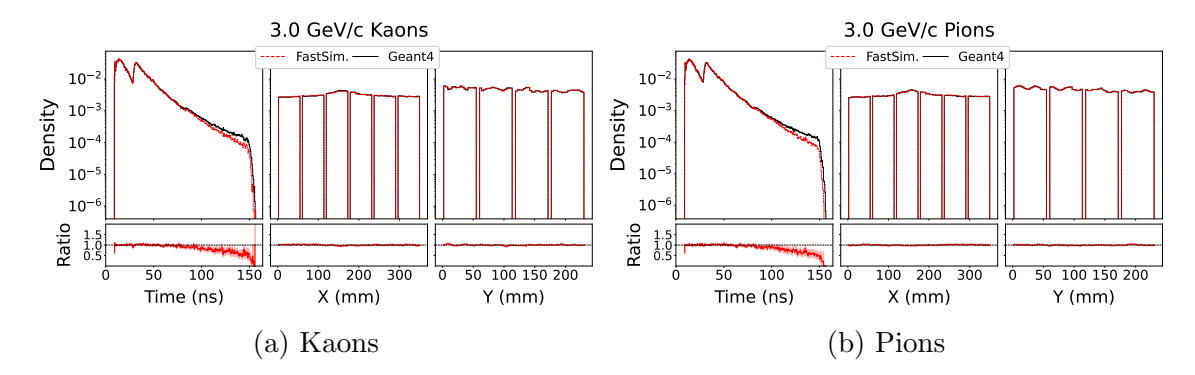


Figure A2: Ratio Plots at 3 GeV/c: Ratio plots for kaons (top) and pions (bottom), using Nucleus sampling and fixed temperature.

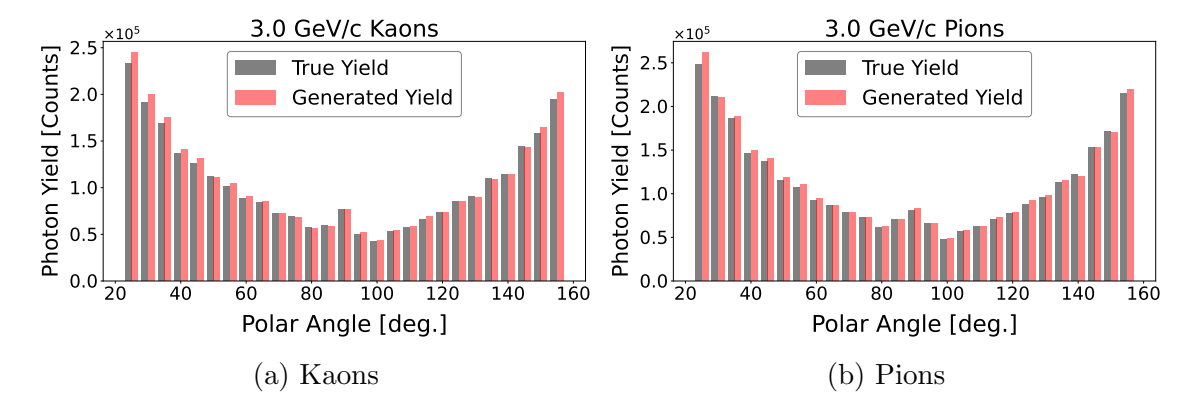


Figure A3: Photon Yield Comparison at 3 GeV/c: Comparison of generated photon yield for kaons (top) and pions (bottom), using Nucleus sampling and fixed temperature.

# Appendix B. Evaluation at $9 \,\mathrm{GeV}/c$

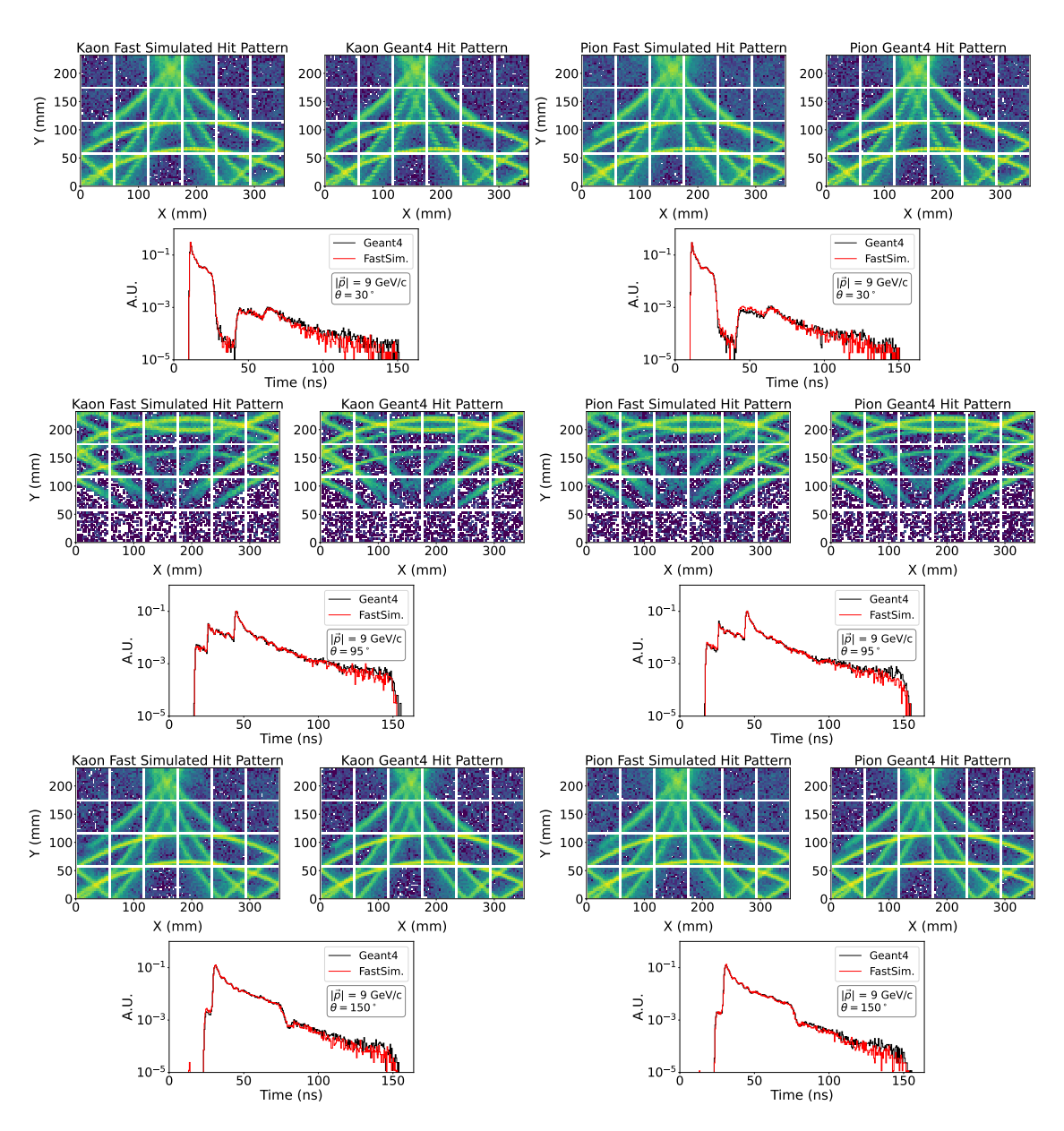


Figure B1: **Fast Simulation at 9 GeV/c:** Fast Simulation of kaons (left column of plots), and pions (right column of plots) at 9 GeV/c and various polar angles, using Nucleus sampling and fixed temperature.

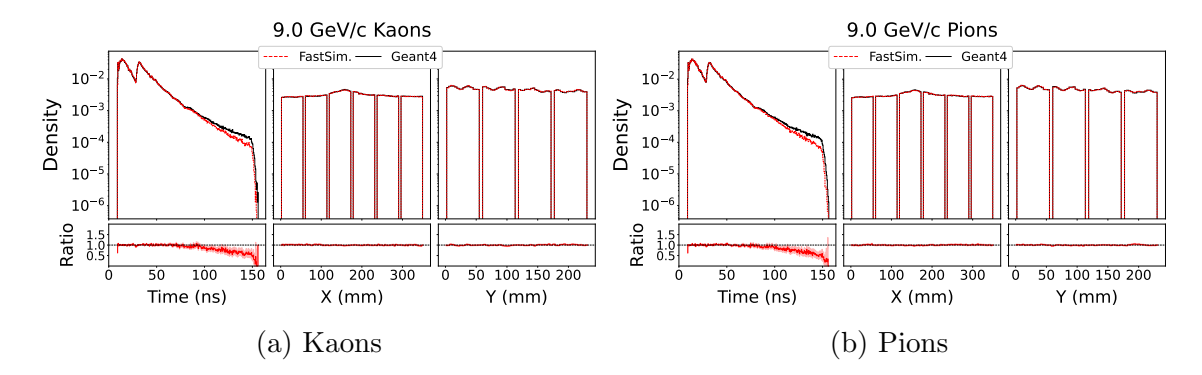


Figure B2: Ratio Plots at 9 GeV/c: Ratio plots for kaons (top) and pions (bottom), using Nucleus sampling and fixed temperature.

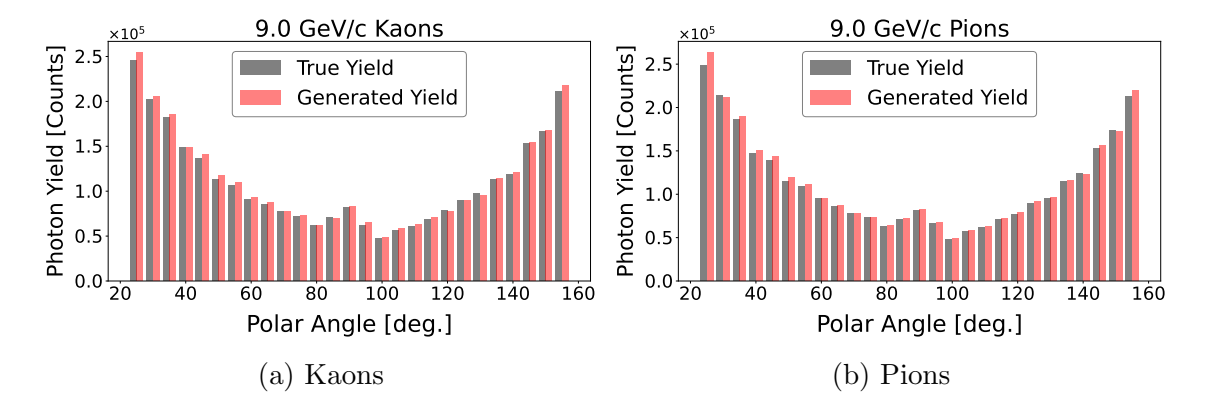


Figure B3: Photon Yield Comparison at 9 GeV/c: Comparison of generated photon yield for kaons (top) and pions (bottom), using Nucleus sampling and fixed temperature.